 doi:10.20944/preprints202009.0582.v1

Article

A Useful Manufacturing Guide for Rotary Piercing Seamless Pipe by ALE Method

Ameen Topa [1,2], Burak Can Cerik [3] and Do Kyun Kim [4,5,*]

[1] Ocean and Ship Technology (OST) Research Group (Department of Civil and Environmental Engineering), Institute of Transportation Infrastructure, PETRONAS University of Technology (UTP), Seri Iskandar, Perak 32610, Malaysia; ameen.topa@utp.edu.my (A.T.)
[2] Department of Maritime Technology, Universiti Malaysia Terengganu, Kuala Terengganu 21300, Malaysia
[3] Department of Naval Architecture and Ocean Engineering, Inha University, Incheon 22212, Korea; bccerik@inha.ac.kr (B.C.C.)
[4] Group of Marine, Offshore and Subsea Technology (MOST), School of Engineering, Newcastle University, Newcastle upon Tyne NE1 7RU, UK
[5] Graduate Institute of Ferrous Technology (GIFT), Pohang University of Science and Technology (POSTECH), Pohang 37673, Korea
* Correspondence: do.kim@ncl.ac.uk (D.K.K.)

Abstract: The development of numerical simulations is potentially useful in predicting the most suitable manufacturing process and ultimately improving product quality. Seamless pipes are manufactured by rotary piercing process in which round bars are fed between two rolls and pierced by a stationary plug. During this process, the material undergoes severe deformation which renders it impractical to be modelled and analysed with conventional finite element methods. In this paper, three dimensional numerical simulations of the piercing process are performed with Arbitrary Lagrangian-Eulerian (ALE) Formulation in LS DYNA software. Details about the material model as well as the elements formulations are elaborated here and mesh sensitivity analysis was performed. The results of the numerical simulations are in good agreement with experimental data found in the literature and the validity of the analysis method is confirmed. The effects of varying workpiece velocity, process temperature, and wall thickness on the maximum stress levels of the product material/pipes are investigated by performing simulations of sixty scenarios. Three dimensional surface plots are generated which can be utilized to predict the maximum stress value at any given combination of the three parameters.

Keywords: Arbitrary Lagrangian-Eulerian (ALE) method; structural analysis; structural design; rotary piercing; seamless pipes; bulk metal forming; FSI

1. Introduction

Metal pipes are categorised into welded pipes and seamless pipes. Welded pipes are commonly manufactured by bending and welding metal sheets, while seamless pipes are produced using the rotary piercing process. It is well recognised that seamless pipe provides additional benefits than welded pipe such as 1) increased pressure ratings, 2) uniformity of shape, and 3) strength under load. Offshore industry especially requires over 30–40 years of design life and robust design of pipeline and riser structures are requested by adopting reliable material, manufacturing process, installation and operation. Many benefits of seamless pipe, i.e., uniformity of shape and fatigue and strength capacity, may allow to secure the higher safety during the operation period of offshore pipeline [1–3] and riser structures [4–6] from the repeated environmental loadings [7–8].

In rotary piercing process, a heated cylindrical workpiece is fed into a plug by the action of two skewed rolls which rotates in the same direction. The rolls are tilted and placed on opposite sides of the workpiece, providing both rotation and translation to the workpiece. As mentioned by Komori

[9], the rolls can be barrel-shaped or cone-shape. Since the invention of the piercing process over a century ago, numerous empirical and analytical studies have been conducted and one of the good studies have been conducted by Komori and Mizuno [10]. Experimental studies on cone-shaped type rotary piercing using lead and wax were performed and a comparison was drawn between two-roll and three-roll cone systems. It was shown that the three-roll cone systems are superior to that of two-roll systems by Khudeyer et al. [11]. The effects of varying the feed angle on the shear strain was studied experimentally using hot steel. Hayashi and Yamakawa [12] found that with larger feed and cross angles, the decrease in the circumferential shear strain is more significant. Moon et al. [13] and Sutcliffe and Rayner [14] conducted experimental work on the rolling process using modelling clay (Plasticine) due to the similarities of its stress strain behaviour with that of metals and because of its malleability and low cost.

Finite Element Analysis (FEA) of metal forming processes was further performed to gather necessary information to properly design and control these processes. In addition, the number of experimental trials can be minimized through exploitation of FEA, which would significantly reduce the product development lead time. Moreover, with the decrease of experimental work, the overall development cost of the product would be reduced. Nowadays, the advancement of powerful computers technology enables the numerical simulations to consider a various physical phenomena during metal processing which include deformation, heat transfer, phase transformation and ductile fracture [15–17].

Two dimensional rigid-plastic finite-element simulation of rotary piercing was performed by Mori et al. [18]. However, the accuracy of the results was low since generalised plane-strain was assumed from the simulation. Three dimensional rigid-plastic finite element analysis was performed by Komori [9]. The number of the elements were limited and the mesh was relatively coarse because large amounts of computational time was required. Berazategui et al. [19] used pseudo-concentrations technique to conduct three dimensional rigid-visoplastic finite-element simulations and a new algorithm was proposed to describe the contact boundary conditions between the tools and the blank. The algorithm was validated with industrial tests of the barrel-type rotary piercing process. However, the numerical analysis of the process was found to be complicated and the computational cost was rather large. Thus, an alternative simplified method was highly required [10]. Shim et al. [20] used rigid-thermoviscoplastic finite element method and conducted simulations with AFDEX 3D software to predict the final shape in better detail. Intelligent re-meshing and tetrahedral elements were used which resulted in increased computational cost. The same method was then used to conduct numerical studies on the Mannesmann effect in the piercing process, as well as to compare between the Diescher's guiding disk and Stiefel's guiding shoe [21, 22].

Lee et al. [23] presented a novel method for adaptive tetrahedral element generation for precision simulation of moving boundary problems such as bulk metal forming. The effects of using tetrahedral solid elements were investigated in a three-dimensional simulation of forging process with AFDEX 3D forging simulator. The predictions of both tetrahedral and standard hexahedral elements were in good agreement with experimental data provided that remeshing technique is employed by Lee et al. [24]. Pater and Kazanacki [25] used Simufact Forming software to analyse the effects of the plug diameter, plug advance, and feed angle on the piercing process. The influence of different plug shapes was further investigated by Skripalenko et al. [26]. ProCAST and QForm commercial software were used for the numerical simulation of piercing aluminium alloy. Jung et al. [27] conducted 3D numerical simulations on the elongation rolling process to study how the rolling speed (rpm) and distance of guide shoes influenced the outer diameter and thickness of the pipe. MSC - SuperForm software was used and automatic re-meshing method of hexagonal elements were implemented. Xiong et al. [28] used the reproducing kernel particle method for the steady and non-steady analysis of bulk forming processes and validated the numerical predictions with experimental measurements. Topa and Shah [29] performed 3D numerical simulations for a forging process with complex tool geometry using Smooth Particle Hydrodynamics (SPH) method. The results were in good agreements with experimental data but the method had poor visual representation of the final geometry. Hah and Youn [30] presented an effective Eulerian approach for bulk metal forming based

Preprints (www.preprints.org) | NOT PEER-REVIEWED | Posted: 24 September 2020 doi:10.20944/preprints202009.0582.v1

on representing boundaries as Non-Uniform Rational B-Spline (NURBS) and the effectiveness of the proposed approach were demonstrated by comparing with other numerical methods. However, this approach had the drawback of a blurred boundary condition imposition.

FEA is based on the concept of discretization. The physical structure is divided into a finite number of elements which has a finite number of degree of freedom. Since the physical structure has infinite degree of freedom, a discretization error exists. This error can be minimised if the object is discretized into more elements. However, this will increase the computational cost. Another drawback of conventional finite element methods is the limitations in modelling fluid-like behaviour, in which there was excessive deformation of the material. Severe deformation may result in mesh entanglement as illustrated in Figure 1. This limits the material flow and reduce the geometric accuracy of the simulations. Therefore, a new formulation called Arbitrary Lagrangian-Eulerian (ALE) was introduced to solve these challenges. In this formulation, mesh movements and material movements are uncoupled, thus reducing the elements distortion. This formulation was proven to be successful in modelling the fluid-like behaviours of materials during bulk metal forming [31–35].

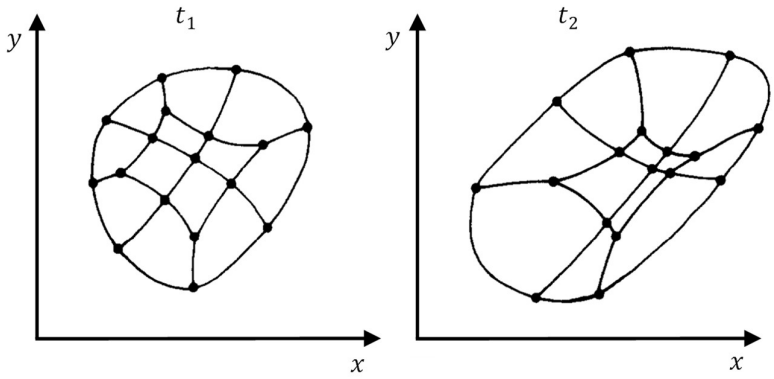

Figure 1. Severe element deformation in finite element analysis [31].

Vavourakis et al. [36] used a decoupled ALE approach for the large deformation modelling of plane-strain elastoplastic problems and the obtained results were validated with limit analysis solutions. The numerical simulations non-Newtonian fluid flow in three dimensional moulding process were performed with ALE method and the capabilities of this method were demonstrated by Wang and Li [37]. ALE formulations was used for the numerical simulation of a complex continuous-type roll-forming process using the in-house finite element code METAFOR and results were in good agreement with classical Lagrange method [38]. Recently, the manufacturing chain including the continuous roll-forming operation, the in-line welding process for closed sections and the post-cut operations was numerically simulated with ALE method by Crutzen et al. [39]. However, validation of the proposed modelling technique was needed as there was no available experimental data in the literature. ALE has proven successful in modelling other areas of metal forming as well. Ducobu et al. [40] adopted ALE formulation and performed a three dimensional numerical simulations of orthogonal cutting operation of Ti6Al4V. The finite element model was validated against experimental data and recommendations on modelling technique were proposed. Avevor et al. [41] analysed the chip formation process in high speed machining of aluminium alloy AA2024–T351 and utilized ALE method in the numerical simulations. The predicted cutting forces was compared to those of experimental work and good agreement was found.

In this paper, the numerical simulations of rotary piercing process were conducted using Arbitrary Lagrangian-Eulerian formulation with LS-DYNA commercial software [42]. The workpiece used in the experiments has a fluid-like behaviour due to its high workability and large deformation during the piercing process. The results of the numerical simulations were then compared to the empirical data available in the literature [9]. The effects of varying the roll velocity, temperature of the raw material, and pipe thickness on the maximum stress values were investigated.

Preprints (www.preprints.org) | NOT PEER-REVIEWED | Posted: 24 September 2020 doi:10.20944/preprints202009.0582.v1

2. Investigation on Seamless Pipe Manufacturing Process by ALE Numerical Simulation Technique

2.1. Simulation Procedure

The stress strain behaviour of Plasticine is similar to that of steel in hot conditions, thus, it is a good substitute for modelling the material behaviour during the piercing process. Apart from lead, which is another choice of material, Plasticine is more commonly used due to its low cost and the simplicity of analysing its material kinematics flow during formation [43,44]. The mechanical properties of standard Plasticine were obtained from previous studies [45–47] which are listed in Table 1. The stress strain curves of Plasticine for different strain rates at room temperature are illustrated in Figure 2.

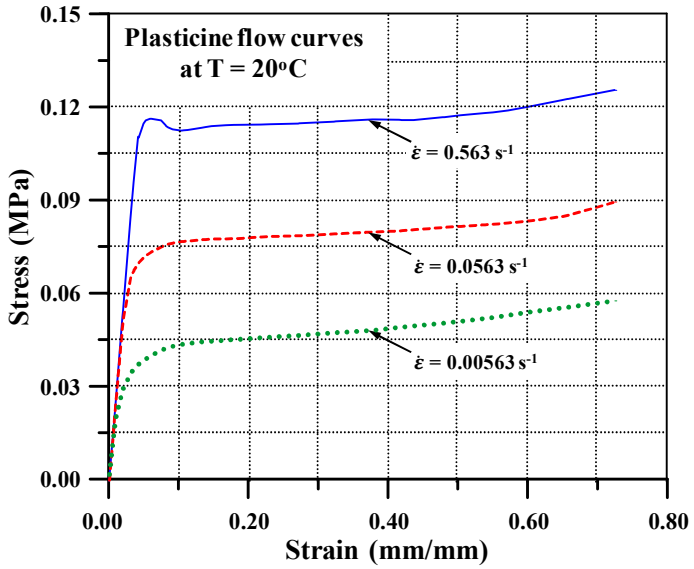

Figure 2. Stress strain curves of Plasticine at room temperature [47].

The tools are assumed to be rigid parts as their deformation is insignificant and out of the scope in the current study. They are modelled with shell elements to minimise computational cost. Material model 27 (PIECEWISE LINEAR PLASTICITY) was used to model the Plasticine material behaviour. In this model, the stress strain curve of the material can be imported to the keyword file to define the relationship between stress and strain. Multiple curves at different strain rates can be used to take into consideration the strain rates effect via stress yield scaling method. Large deformation will cause an increase in the temperature and soften the material properties. However, due to the high velocity of the process, it was assumed that changes to temperature was minimum and there was insufficient time for heat transfer to occur between the workpiece and the tools. Thus, the process is simplified to an isothermal and adiabatic system.

Table 1. Mechanical properties of Plasticine.

Property	Unit	Value
Density	kg/m^3	1800
Young's Modulus	MPa	42.5
Yield Stress	MPa	0.18
Poisson's ratio	-	0.434

The workpiece is a cylindrical billet with an original diameter of 45 mm, which is fed between two tilted coned-shaped rolls with a feed angle of 9 degrees (°). The rolls have a maximum diameter of 292 mm and the distance between their axes of rotation is 330 mm. Thus, the minimum roll gap is 38 mm. The plug advance is 25 mm and its maximum diameter is 33 mm. These piercing process

Preprints (www.preprints.org) | NOT PEER-REVIEWED | Posted: 24 September 2020 doi:10.20944/preprints202009.0582.v1

parameters are listed in Table 2. These parameters were made identical to those previously reported by Komori [9] for comparison purposes. The schematic diagrams and simulation model of the process are shown in Figures 3 and 4, respectively.

Table 2. Parameters of rotary piercing process.

Parameter	Value	Parameter	Value
Initial workpiece diameter (mm)	45	Distance between roll axes (mm)	330
Minimum roll gap (mm)	38	Feed angle (°)	9
Maximum plug diameter (mm)	33	Entrance face angle (°)	3.5
Plug advance (mm)	25	Exit face angle (°)	3
Guide shoe diameter (mm)	47	Roll velocity (mm/s)	5

In order to use ALE formulation, the meshes of the initial workpiece geometry and the surrounding space must have merged nodes at their shared boundaries. Solid Element Formulation 12 was used which stands for 1-point integration element with single material and void. In this element formulation, two overlapping meshes exist. The first is a fixed or movable background mesh while the second mesh is connected to the material which flows through the first mesh. This process can be visualized as two steps. In one step, the material undergoes deformation as in standard finite element methods. In the next step, the element's state variables such as stress, strain, and velocity are re-mapped or distributed back onto the mesh. Figure 5 is a visualization of material 'flowing' in the ALE formulation. As the workpiece was largely deformed during the process, it was modelled with this element formulation and solid hexagonal elements were used.

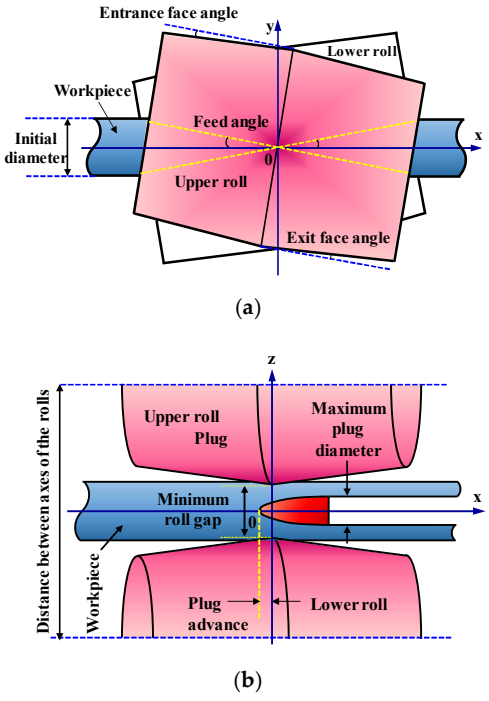

Figure 3. Schematic diagram of the piercing process.

Preprints (www.preprints.org) | NOT PEER-REVIEWED | Posted: 24 September 2020 doi:10.20944/preprints202009.0582.v1

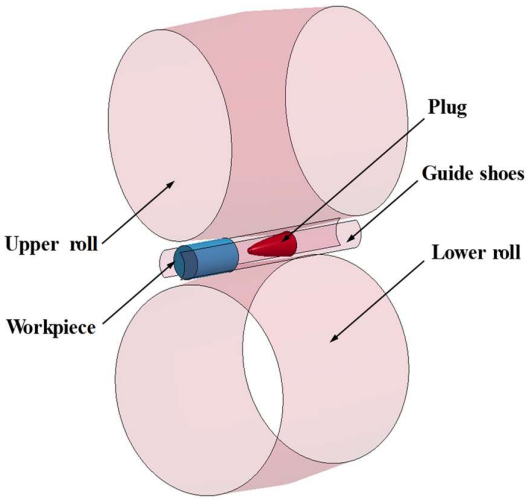

Figure 4. FEA model of tools and workpiece.

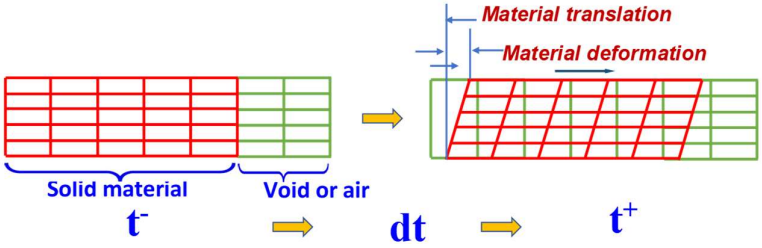

Figure 5. Solid material deforms and translates inside the fixed mesh [48].

The interactions (or coupling) between the ALE parts (workpiece) and the Lagrangian parts (tools) are materialized with CONSTRAINED LAGRANGE IN SOLID command. The code will search for the penetrations between the abovementioned parts and apply coupling forces to redistribute the material back into both meshes. Penalty coupling algorithm was used. Improper input of this command will cause leakage problem in which the ALE parts will pass through the tools. Table 3 summarizes the input parameters for this command.

Table 3. Input values for the coupling definition.

Parameter	Description	Value
NQUAD	Number of quadrature points	3
CTYPE	Coupling type	4
DIREC	Coupling direction	2
PFAC	Penalty factor	0.1
FRCMIN	Minimum volume fraction for coupling activation	0.4
ILEAK	Leakage control	2
PLEAK	Leakage control penalty factor	0.1
PFACMM	Mass-based penalty stiffness factor	3

2.2. Mesh Sensitivity Study

The accuracy of any FEA analysis depends on many factors including the mesh size. Commonly, a coarse mesh is used in the preliminary stages of the studies in order to get quick results. Finer mesh is used at later stages to obtain more accurate results. However, models with more number of elements have higher computational cost. Sensitivity analysis is performed to obtain the optimal mesh size.

Preprints (www.preprints.org) | NOT PEER-REVIEWED | Posted: 24 September 2020 doi:10.20944/preprints202009.0582.v1

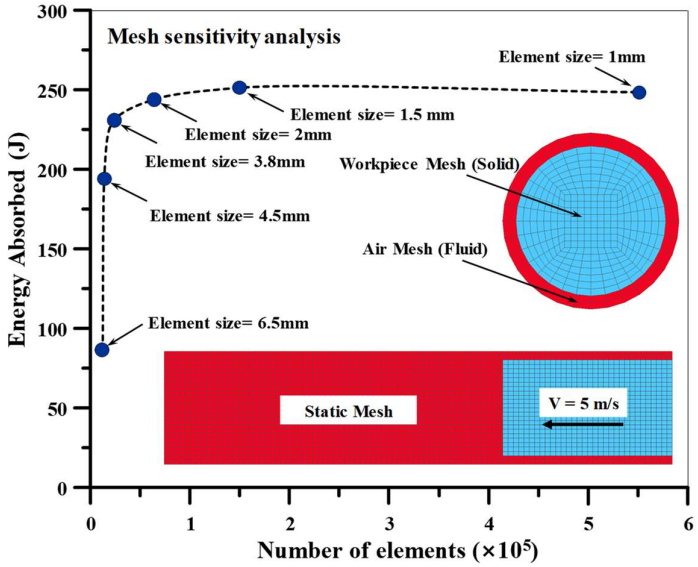

Figure 6. Mesh sensitivity analysis result.

Sensitivity analysis was performed for six different mesh sizes. Figure 6 shows the convergence of maximum energy absorbed as the number of elements was increased. Furthermore, the simulations with more than 54,612 elements (average mesh size of 2 mm) resulted in slight changes in the energy absorbed values. By roughly tripling the number of elements to 140,600, only a slight change of 3.11% was reported. Therefore, 2 mm mesh size was selected as the optimum size for subsequent simulations. Figure 7 demonstrates the final obtained result from the process. The selected mesh size generated a smooth representation of the geometry of the pipe compared to a coarser mesh.

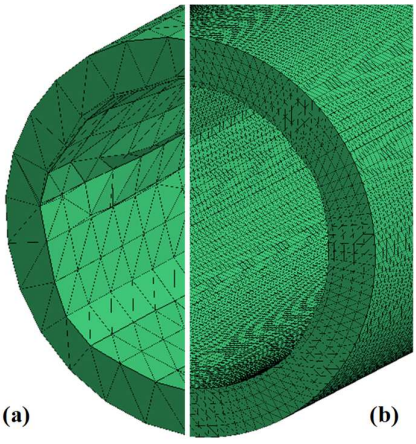

Figure 7. Fine mesh results in smoother final shape: (**a**) 4,650 elements vs. (**b**) 54,612 elements.

2.3. Numerical Simulation Results and Validation

The deformation of the workpiece as it is compressed by the rollers and pierced by the plug is shown in Figure 8. This illustrates how the ALE formulation is capable of capturing the large deformation of the workpiece. Contour plots of the equivalent von Mises stress in Figure 9 reveal that the maximum stress values are not located on the external surface of the pipe wall, but rather are located near the plug tip. This is due to the stress concentration at this region as the material is being pushed towards the small area of the plug tip. Furthermore, the friction between the workpiece and the plug will contribute to the shearing of the material as it flows tangentially to the plug surface.

Preprints (www.preprints.org) | NOT PEER-REVIEWED | Posted: 24 September 2020 doi:10.20944/preprints202009.0582.v1

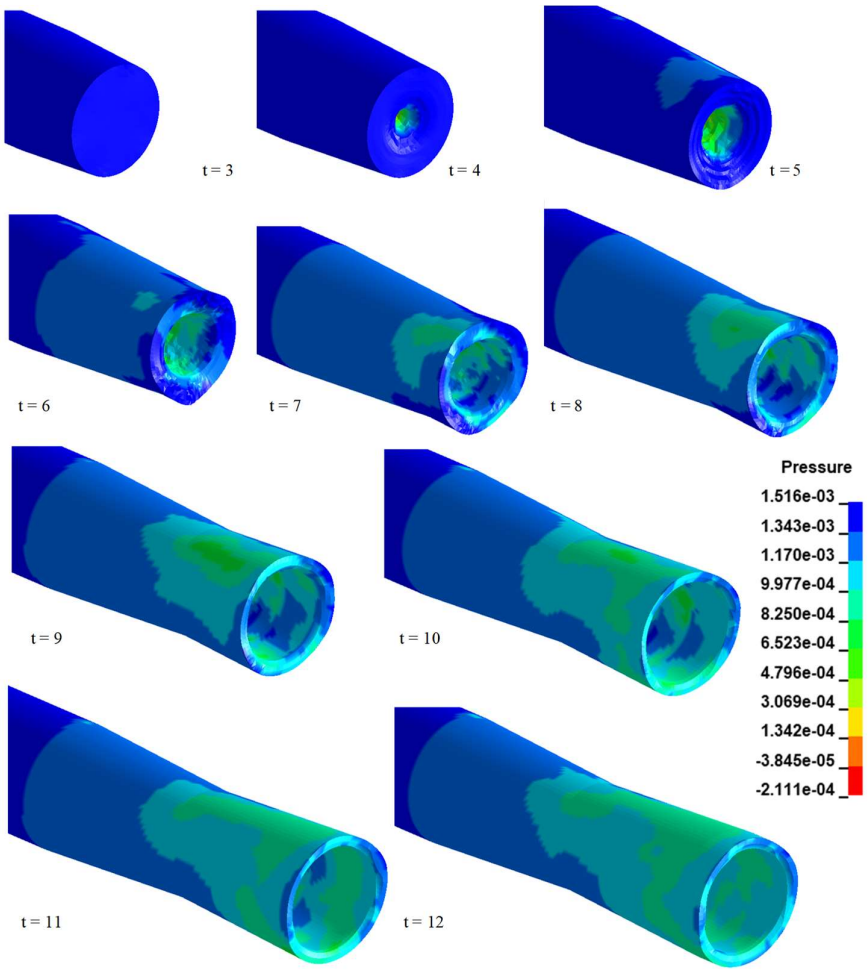

Figure 8. Contour plots of pressure showing the development of the pipe geometry.

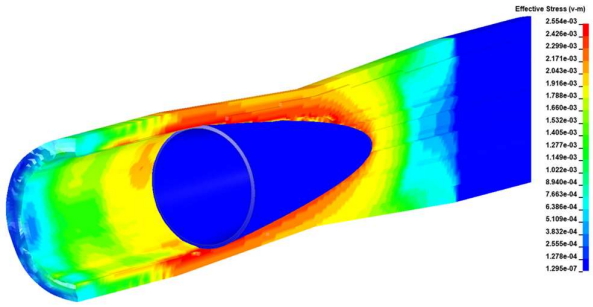

Figure 9. Stress concentration around the plug.

Figure 10 shows the volumetric strain contours at different cross sectional views. It was observed that strain values increased as the material deforms and the inner diameter became bigger. Throughout the process, the strain values were axisymmetric. Investigation of Lode parameter plot reveals it equals to zero around the area of contact with plug tip. This state corresponds to a shear stress combined with a hydrostatic stress state which indicates that the material is most susceptible to ductile fracture [49]. Therefore, the plug shape plays an important role in the reliability of the final product.

Preprints (www.preprints.org) | NOT PEER-REVIEWED | Posted: 24 September 2020 doi:10.20944/preprints202009.0582.v1

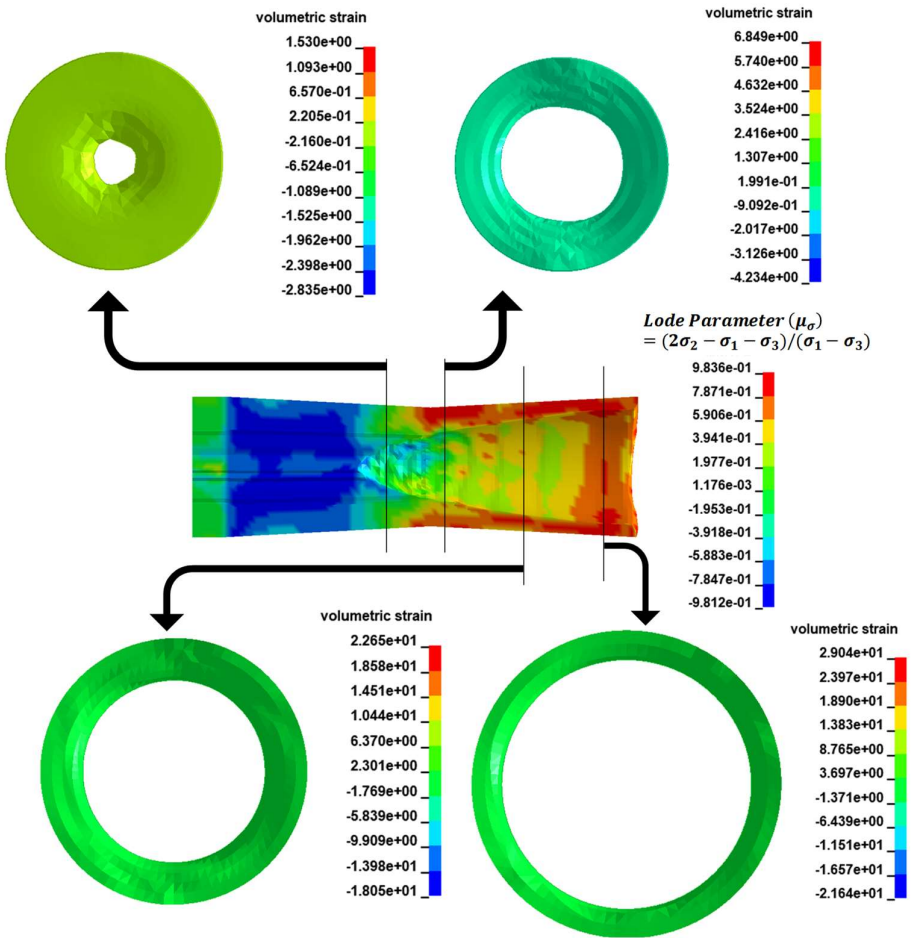

Figure 10. Side cross sectional view shows Lode parameter and frontal cross section views at different locations.

The results revealed some imperfections in the inner diameter of the pipe. As shown in Figure 11, the final shape is represented by the green solid while the red dotted line indicated a perfect circle. This demonstrated the capability of the ALE method to describe and predict defects in the final shape. Due to these imperfections, further processes are usually required to treat the pipe and improve its dimensions. The outer diameter had no significant imperfections due to the existence of guide shoes which assisted in achieving the final outer dimeter.

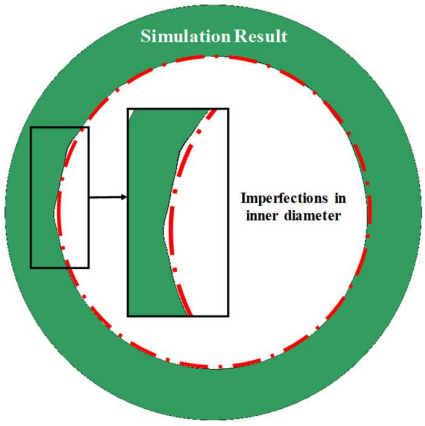

Figure 11. Imperfections in the inner diameter.

Preprints (www.preprints.org) | NOT PEER-REVIEWED | Posted: 24 September 2020 doi:10.20944/preprints202009.0582.v1

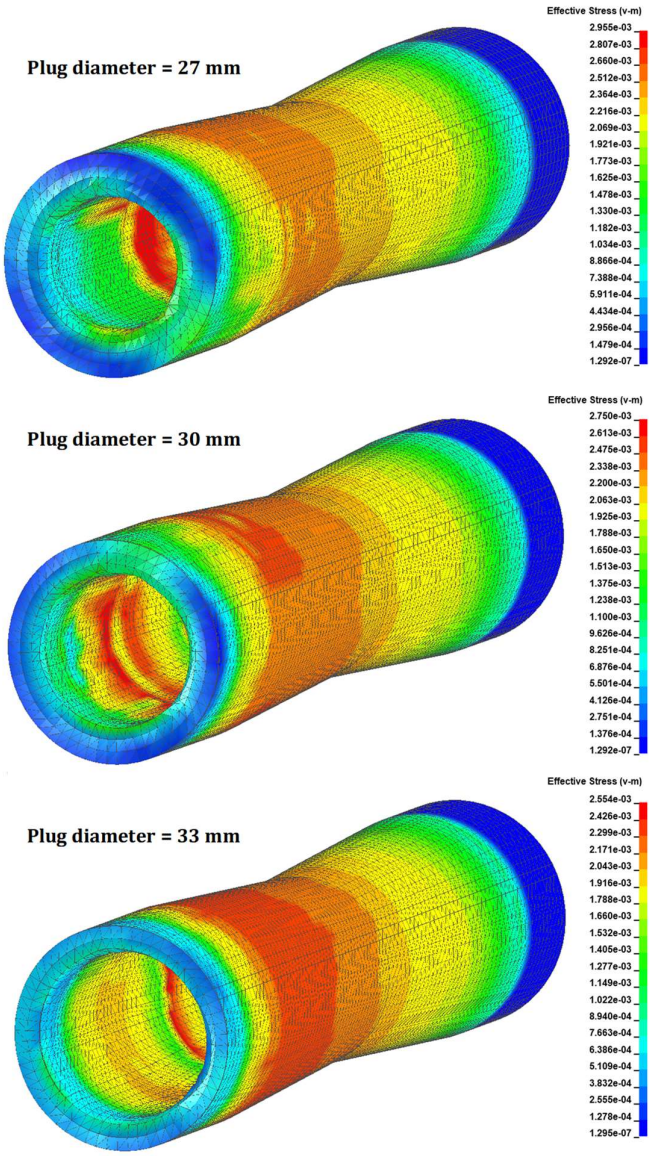

Figure 12. Rotary piercing with different maximum plug diameters.

For validation purposes, the numerical simulations were performed at two additional maximum plug diameters: 30 mm and 27 mm as shown in Figure 12. The average values of the inner and other diameters were measured in each simulation. Varying the maximum plug diameter affected the inner diameter of the final pipe geometry but had little influence on the outer diameter. Comparisons between the results obtained and experimental data revealed a good positive correlation with a low percentage of error (2.11%) as illustrated in Figure 13. For further validation of the FEA model, additional simulations were performed at different feed angles: 6, 9, and 12 degrees. The variation of the feed angle had insignificant influence on the pipe's final dimensions. In all three cases, the results of the final diameters matched well with previous data as shown in Figure 14.

As seen in Figure 12, with smaller plug diameters, larger final thickness is achieved. For plug values of 33, 30, and 27 mm, the outer diameter to thickness ratios are 7.5, 6.0, and 5.0, respectively. The outer diameter is kept constant throughout this study and the D/t ratio is varied by changing the plug diameter.

Preprints (www.preprints.org) | NOT PEER-REVIEWED | Posted: 24 September 2020 doi:10.20944/preprints202009.0582.v1

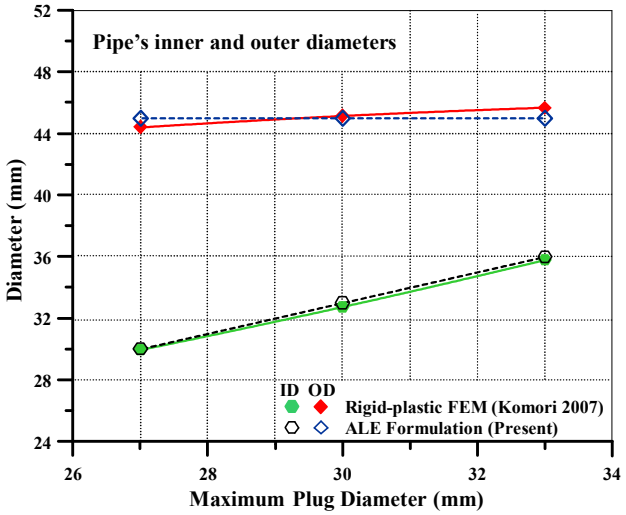

Figure 13. Pipe average diameter versus maximum plug diameter.

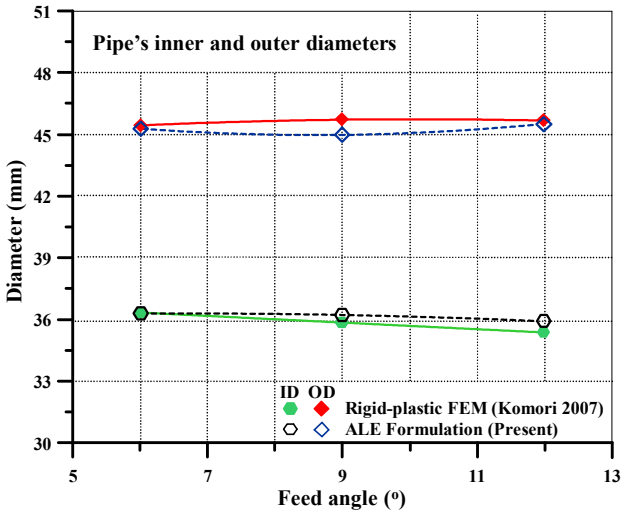

Figure 14. Pipe average diameter versus feed angle.

3. Sensitivity Analysis by Considering the Effect of Velocity, the Temperature and the Maximum Plug Diameter

The effects of workpiece velocity, material temperature, and maximum plug diameter in different combinations were investigated numerically by performing a total of sixty scenarios. The influence of each variable on the maximum stress values was investigated separately by fixing the other two variables. The simulation scenarios were generated by three values of velocity, four values of maximum plug diameter, and five values of material temperature, as listed in Table 4. The results of three selected scenarios are illustrated in Figure 15.

Preprints (www.preprints.org) | NOT PEER-REVIEWED | Posted: 24 September 2020 doi:10.20944/preprints202009.0582.v1

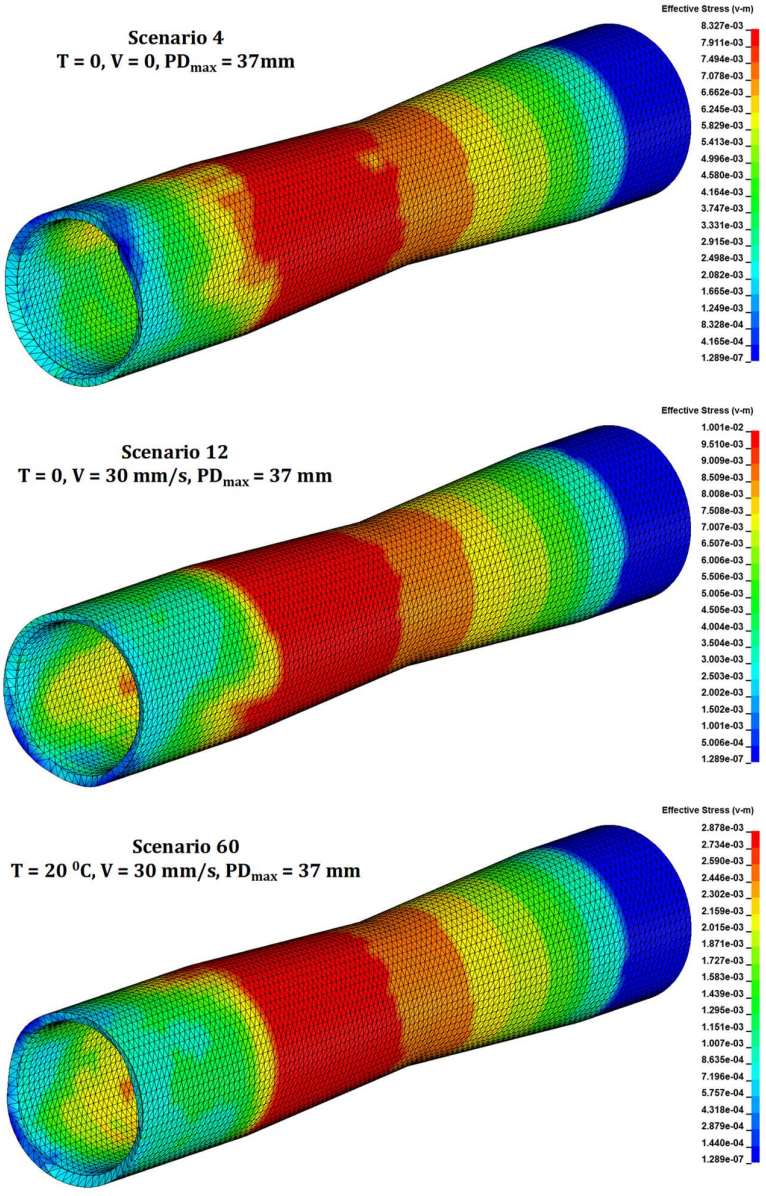

Figure 15. Stress contour plots of scenarios no. 4, 12, and 60.

Preprints (www.preprints.org) | NOT PEER-REVIEWED | Posted: 24 September 2020 doi:10.20944/preprints202009.0582.v1

Table 4. Summary of the 60 simulation scenarios.

SN	T	V	PD_{max}	SN	T	V	PD_{max}	SN	T	V	PD_{max}
1	0	5	27	**21**	5	30	27	**41**	15	15	27
2	0	5	30	**22**	5	30	30	**42**	15	15	30
3	0	5	33	**23**	5	30	33	**43**	15	15	33
4	0	5	37	**24**	5	30	37	**44**	15	15	37
5	0	15	27	**25**	10	5	27	**45**	15	30	27
6	0	15	30	**26**	10	5	30	**46**	15	30	30
7	0	15	33	**27**	10	5	33	**47**	15	30	33
8	0	15	37	**28**	10	5	37	**48**	15	30	37
9	0	30	27	**29**	10	15	27	**49**	20	5	27
10	0	30	30	**30**	10	15	30	**50**	20	5	30
11	0	30	33	**31**	10	15	33	**51**	20	5	33
12	0	30	37	**32**	10	15	37	**52**	20	5	37
13	5	5	27	**33**	10	30	27	**53**	20	15	27
14	5	5	30	**34**	10	30	30	**54**	20	15	30
15	5	5	33	**35**	10	30	33	**55**	20	15	33
16	5	5	37	**36**	10	30	37	**56**	20	15	37
17	5	15	27	**37**	15	5	27	**57**	20	30	27
18	5	15	30	**38**	15	5	30	**58**	20	30	30
19	5	15	33	**39**	15	5	33	**59**	20	30	33
20	5	15	37	**40**	15	5	37	**60**	20	30	37

Note: SN = Scenario number, T = material temperature (°C), V = velocity (mm/s), and PD_{max} = maximum plug diameter (mm).

It was found that increasing the workpiece velocity resulted in higher stress levels. Referring to Figure 15, the first two results are for scenarios 4 and 12, respectively. In these two cases, all the parameters were identical except for the velocity of the workpiece. At 5 mm/s, the maximum stress was 8.33 MPa while at an increased velocity of 30 mm/s, the maximum stress reached 10.01 MPa. Since the effects of strain rates on Plasticine material is similar to those of steel, the trend of the results shown in Figure 16 can be generalised to the piercing of steel pipes. Data in this figure was generated with the maximum plug diameter constant at 37 mm while the velocity and temperature were varied. The increase of maximum stress values due to the velocity variation at 20°C was less compared to 0°C. Therefore, it can be concluded that the effects of strain rate towards the pipes are more significant at lower temperatures. Preheating the specimen is preferred as it increases the malleability and workability of the material.

Referring again to Figure 15, the middle and last contour plots corresponds to scenarios 12 and 60, respectively. The only parameter changed in these two scenarios was the temperature. Increasing the temperature from 0°C to 20°C resulted in dropping the maximum stress from 10.01 MPa to 2.88 MPa. This is due to a phenomenon called thermal softening. The general influence of material temperature on the maximum stress values is illustrated by the curves in Figure 17. Each curve represents the maximum stress outcome at a different maximum plug diameter. At higher temperatures, the material becomes softer and more malleable. Therefore, the material provided less resistance to deformation, which in turn yielded less stress values. It was also observed that the vertical distance between each curve decreased as the temperature raised. Hence, it was concluded that changes in the tool geometry, which was represented by the maximum plug diameter, had less effects on the stress values at higher temperatures. Thus, for more complex geometries, it would be preferable to increase the temperature of the workpiece material.

Preprints (www.preprints.org) | NOT PEER-REVIEWED | Posted: 24 September 2020 doi:10.20944/preprints202009.0582.v1

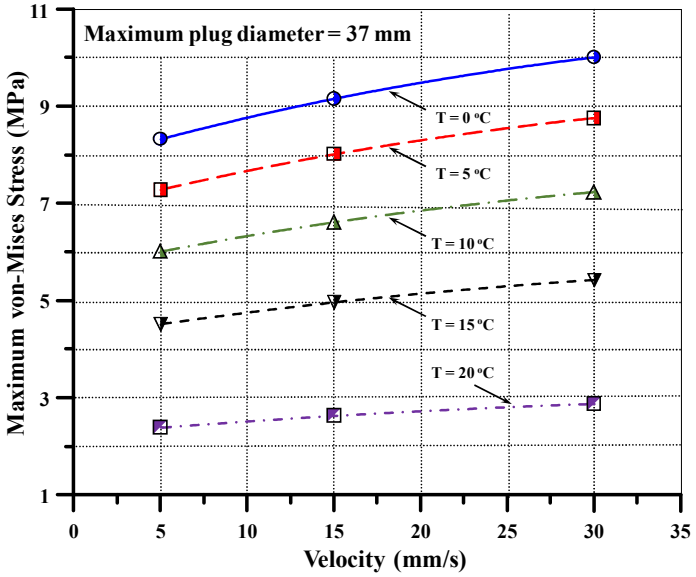

Figure 16. Effect of velocity on maximum von Mises stress at PD_{max} = 37 mm.

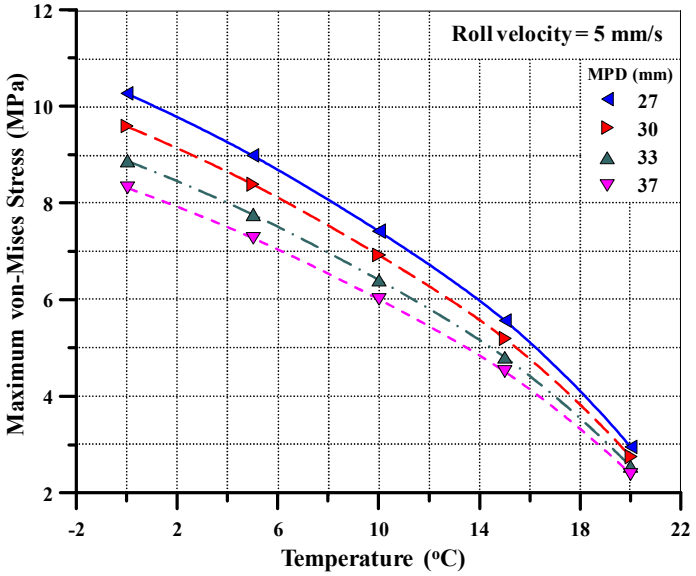

Figure 17. Effect of material temperature on maximum von Mises stress at V = 5 mm/s.

Lastly, the effect of the plug diameter was investigated. The stress contours of three cases are illustrated in Figure 12. With a smaller plug diameter of 27 mm, the maximum stress reached 2.96 MPa, and at a larger plug diameter of 33 mm, the value slightly dropped to 2.54 MPa. It was evident from Figure 18 that increasing the maximum plug diameter resulted in less stress levels. This was due to the change in the curvature of the plug head. For plugs with lower diameters, the curvature of its head must be increased. This 'sharper' head generates higher stresses towards the workpiece material by pressing against it. Reducing the velocity of the workpiece would marginally help in reducing the stress levels.

Preprints (www.preprints.org) | NOT PEER-REVIEWED | Posted: 24 September 2020 doi:10.20944/preprints202009.0582.v1

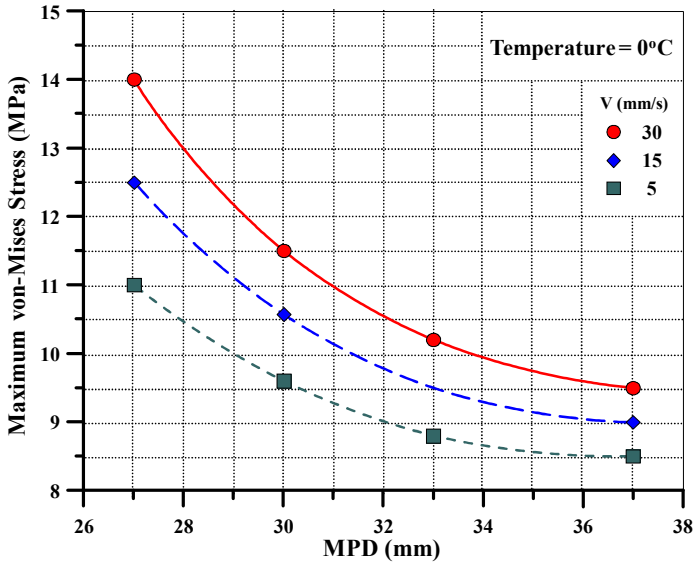

Figure 18. Effect of maximum plug diameter on maximum von Mises stress at T = 0°C.

Combining the findings from the previous figures, the effects of the three variables on the maximum von Mises stress can be summarised as follows: the increase in temperature and plug diameter resulted in lower stress values while increasing the velocity increased the stresses. A three dimensional surface plot which depicts the combined effects is illustrated in Figure 19. This plot can be utilized to predict the maximum stress values at any combination of the three main parameters: material temperature, maximum plug diameter, and workpiece velocity, within the respective limits of each variable considered in this study.

Polynomial fitting equations of the third degree with ten coefficients were generated for the surface plots as follows:

$$\sigma_{von\ Mises} = \sum_{i=0}^{3}\sum_{j=0}^{3} C_{ij}x^i y^j \,, for\ (i+j) \le 3$$
$$= C_{00} + C_{10}\,x + C_{01}\,y + C_{11}\,xy + C_{20}\,x^2 + C_{20}\,y^2 + C_{21}\,x^2y + C_{12}\,xy^2 + C_{30}\,x^3 + C_{03}\,y^3 \quad (1)$$

where, PD_{max} is the maximum plug diameter ($27 \le PD_{max} \le 37$), T is the material temperature ($0 \le T \le 20$), and C is the coefficient of each term in the equation. The coefficients of each fitting equations and their goodness of fit are listed in Tables 5 and 6, respectively.

Preprints (www.preprints.org) | NOT PEER-REVIEWED | Posted: 24 September 2020 doi:10.20944/preprints202009.0582.v1

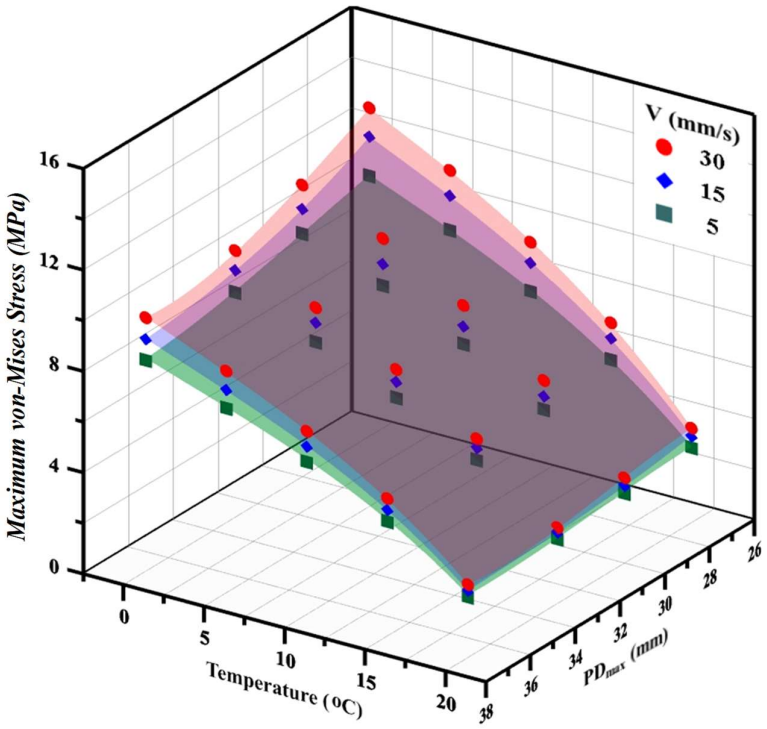

Figure 19. Surface plots illustrating the effects of the variables on the maximum von Mises stress.

Table 5. Determined coefficients of proposed equation.

Surface	C	Value	C	Value
V = 5 mm/s	C_{00}	-13.45	C_{11}	0.02057
	C_{10}	2.82	C_{21}	-0.0002623
	C_{01}	-0.6224	C_{12}	0.0001563
	C_{20}	-0.1031	C_{30}	0.001158
	C_{02}	-0.003655	C_{03}	-0.0002983
V = 15 mm/s	C_{00}	54.73	C_{11}	0.05132
	C_{10}	-3.005	C_{21}	-0.0007234
	C_{01}	-1.154	C_{12}	0.0002157
	C_{20}	0.06465	C_{30}	-0.0004516
	C_{02}	-0.005454	C_{03}	-0.00033
V = 30 mm/s	C_{00}	-28.33	C_{11}	0.06595
	C_{10}	5.272	C_{21}	-0.0009622
	C_{01}	-1.391	C_{12}	0.0003002
	C_{20}	-0.2039	C_{30}	0.002417
	C_{02}	-0.008803	C_{03}	-0.0003383

Preprints (www.preprints.org) | NOT PEER-REVIEWED | Posted: 24 September 2020 doi:10.20944/preprints202009.0582.v1

Table 6. Goodness of fit for each surface plot equation.

Surface	Goodness of Fit	Value
V = 5 mm/s	SSE	0.01303
	R^2	0.9999
	Adjusted R^2	0.9998
	RMSE	0.0361
V = 15 mm/s	SSE	0.01488
	R^2	0.9999
	Adjusted R^2	0.9998
	RMSE	0.03585
V = 30 mm/s	SSE	0.4139
	R^2	0.9998
	Adjusted R^2	0.9995
	RMSE	0.06434

Note: SSE = Sum of Squared Errors, R^2 = Coefficient of Determination, and RMSE = Root Mean Square Error.

To investigate the maximum stress values at any given velocity between the upper and lower limits (5 mm/s and 30 mm/s, respectively), interpolation was performed on the 10 coefficients of the surface equation. The coefficients C_{01}, C_{02}, C_{21}, and C_{03} are negatively correlated to the velocity while C_{11} and C_{12} have a positive correlation. The remaining coefficients: C_{00}, C_{10}, C_{20} and C_{30} have a maximum/minimum values within the range of velocity investigated. The curves in Figure 20 can be used to determine the values of the coefficients.

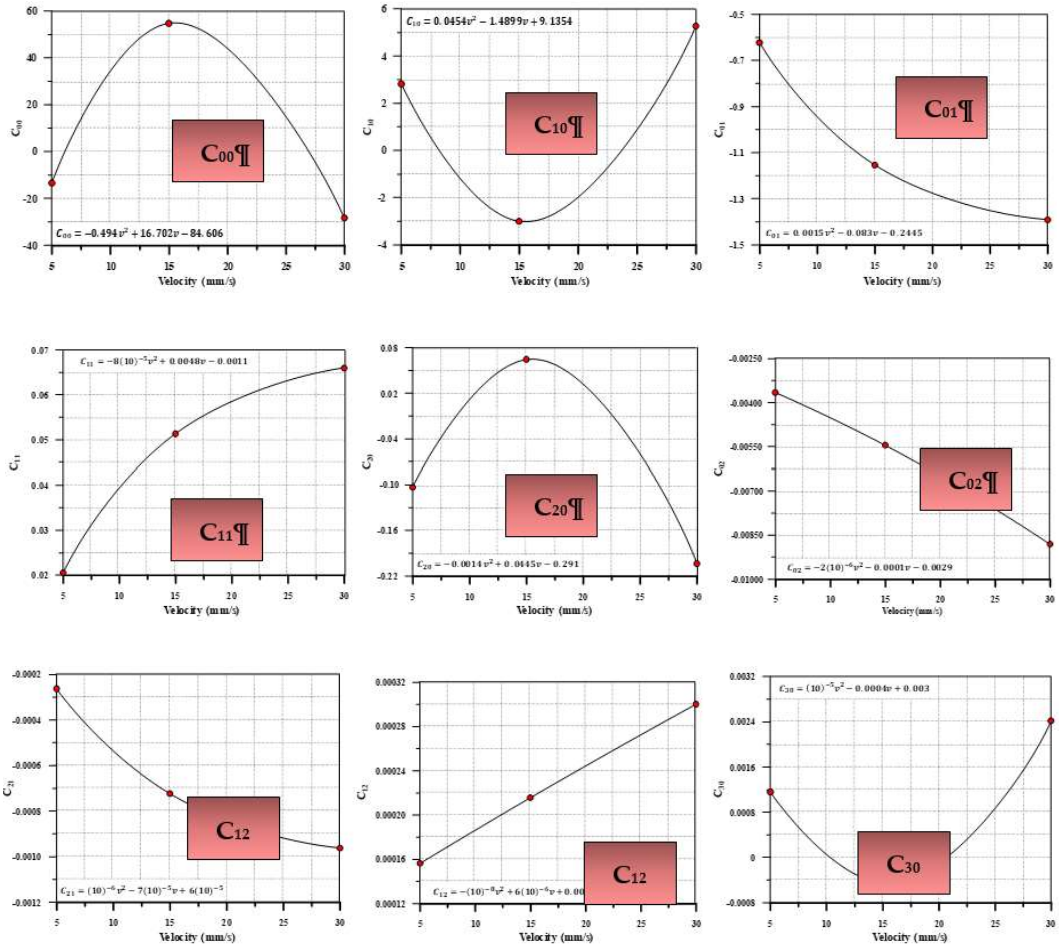

Preprints (www.preprints.org) | NOT PEER-REVIEWED | Posted: 24 September 2020 doi:10.20944/preprints202009.0582.v1

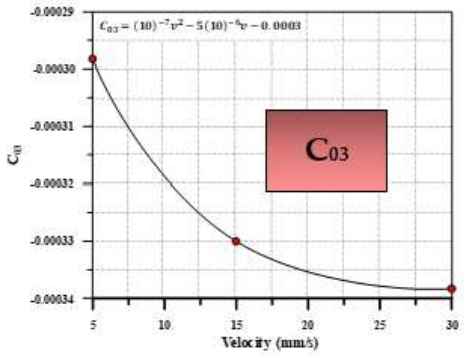

Figure 20. Interpolations of the coefficients of the proposed equation.

This paper proposes the use of ALE formulation to perform three dimensional finite element analysis of the rotary piercing process of Plasticine material. The capability of the method to describe the large deformation and fluid-like behaviour of the workpiece was shown and the results of the numerical simulations were in good agreement with the experimental data. The validated FEA model was utilised to study the influence of the three main variables consisting of, material temperature, maximum plug diameter, and piercing velocity. Three dimensional surface plots were generated to describe the relationship between the three variables and maximum von Mises stress in the material.

The developed FEA model with ALE formulation gave better results than conventional FEA methods as it does not suffer from the limitations of the latter such as mesh distortion and elements entanglement. However, it requires more computational time as it necessitates modelling the surrounding space and thus the model will be inherently larger in size. Also, the interaction between the ALE material and different parts depends on the relative mesh size and inadequate modelling of this coupling will result in a leakage problem which is very common problem in modelling with ALE formulation. The optimal parameters for the coupling keyword is obtained through trial and error as it varies from one case to another.

It was found that the piercing velocity has a proportional correlation with the maximum stress values while workpiece temperature and plug diameter have the opposite effect. However, further numerical simulations are necessary if the values of any of the three variables are not within the limited range of this study. These relationships can be generalized to the piercing of the steel due to the resemblance of the stress strain behaviour of Plasticine to that of steel at elevated temperatures. However, benchmarking analysis with empirical data of steel piercing process are required.

This work focused on the rotary piercing of Plasticine workpiece materials and failure analysis and crack initiation were not considered. Future work will be to investigate the piercing of full-scale metal pipe at elevated temperatures. The numerical simulation will then be performed with ALE formulation to predict the critical stress and strain values, which may result in defective products with poor structural integrity. Additionally, the ductile fracture criteria may be coupled with the simulation to detect the formation of micro cracks which cannot be visualised by FEA simulations.

Author Contributions: Conceptualization, A.T. and D.K.K.; methodology, A.T. and D.K.K.; software, A.T.; validation A.T. and B.C.C.; formal analysis, A.T. and B.C.C.; investigation, A.T., B.C.C. and D.K.K.; writing—original draft preparation, A.T.; writing—review and editing, B.C.C. and D.K.K.; All authors have read and agreed to the published version of the manuscript.

Acknowledgments: Authors appreciate kind supports from POSTECH (Korea), UTP (Malaysia), and Newcastle University (UK). This study was undertaken at Ocean and Ship Technology (OST) at Universiti Teknologi PETRONAS. This research was supported by the Technology Innovation Program (Grant No.: 10053121 and 10051279) funded by the Ministry of Trade, Industry & Energy (MI, Korea). The authors would also like to thank for the great support of POSTECH, Korea. Part of this study has been presented in International Conference on Civil, Offshore, and Environmental Engineering (ICCOEE2018), 13-14 August, Kuala Lumpur, Malaysia and published in MATEC (https://doi.org/10.1051/matecconf/201820306016).

Funding: This study was supported by Technology Innovation Program (Grant No.: 10053121 and 10051279) funded by the Ministry of Trade, Industry & Energy (MI, Korea).

Conflicts of Interest: The authors declare no conflict of interest.

References

1. Yu, S.Y.; Choi, H.S.; Park, K.S.; Kim, Y.T.; Kim, D.K. Advanced procedure for estimation of pipeline embedment on soft clay seabed. *Structural Engineering and Mechanics* **2013**, 62, 381-389.
2. Mohd H.M.; Kim, D.K.; Kim, D.W.; Paik, J.K. A time-variant corrosion wastage model for subsea gas pipelines. *Ships and Offshore Structures* **2014**, 9, 161-176.
3. Yu, S.Y.; Choi, H.S.; Lee, S.K.; Do, C.H.; Kim D.K. An optimum design of on-bottom stability of offshore pipelines on soft clay. *International Journal of Naval Architecture and Ocean Engineering* **2017**, 5, 598-613.
4. Park, K.S.; Kim, Y.T.; Kim, D.K.; Yu, S.Y.; Choi, H.S. A new method for strake configuration design of steel catenary risers. *Ships and Offshore Structures* **2016**, 11, 385-404.
5. Kim, D.K.; Wong, E.W.C.; Lekkala, M.R. A parametric study on fatigue of a top-tensioned riser subjected to vortex-induced vibrations. *Structural Monitoring and Maintenance* **2019**, 6, 365-387.
6. Kim, D.K.; Incecik, A.; Choi, H.S.; Wong, E.W.C.; Yu, S.Y.; Park, K.S. A simplified method to predict fatigue damage of offshore riser subjected to vortex-induced vibration by adopting current index concept. *Ocean Engineering* **2018**, 157, 401-411.
7. Wong, E.W.C.; Kim, D.K. A simplified method to predict fatigue damage of TTR subjected to short-term VIV using Artificial Neural Network. *Adv. Eng. Softw.* **2018**, *126*, 100–109.
8. Kim, D.K.; Wong, E.W.C.; Lee, E.B.; Yu, S.Y.; Kim, Y.T. A method for the empirical formulation of current profile. *Ships and Offshore Structures* **2018**, 14, 176-192.
9. Komori, K. Simulation of Mannesmann piercing process by the three-dimensional rigid-plastic finite element method. *International Journal of Mechanical Sciences* **2005**, 47, 1838-1853.
10. Komori, K.; Mizuno, K. Study on plastic deformation in cone-type rotary piercing process using model piercing mill for modeling clay. *Journal of Materials Processing Technology* **2009**, 209, 4994-5001.
11. Khudeyer, W.A.; Barton, D.C.; Blazynski, T.Z. A comparison between macroshear redundancy and loading effects in 2- and 3-roll rotary tube cone piercers. *Journal of Material Processing Technology* **1997**, 65, 191-202.
12. Hayashi, C.; Yamakawa, T. Influence of feed and cross angle on rotary forging effects and redundant shear deformations in rotary piercing process. *Iron and Steel Institute of Japan International* **1997**, 37, 146-152.
13. Moon, Y.H.; Chun, M.S.l; Yi, J.J.; Kim, J.K. Physical modeling of edge rolling in plate mill with plasticine. *Steel Research* **1993**, 64, 557-563.
14. Sutcliffe, M.P.F.; Rayner, P.J. Experimental measurements of load and strip profile in thin strip rolling. *International Journal of Mechanical Science* **1998**, 40, 887-899.
15. Rowe, G.W.; Strugess, C.N.; Hartley, P.; Pillinger, I. *Finite-element plasticity and metal forming analysis*; Cambridge University Press: Cambridge, UK, 1991.
16. Hawryluk, M.; Jakubik J. Analysis of forging defects for selected industrial die forging process. *Engineering Failure Analysis* **2016**, 59, 396-409.
17. Guo, Z.; Lasne, P.; Saunders, N.; Schillé J-.P. Introduction of materials modelling into metal forming simulation. *Procedia Manufacturing* **2018**, 15, 372-380.
18. Mori, K.; Yoshimura, H.; Osakada, K. Simplified three-dimensional simulation of rotary piercing of seamless pipe by rigid-plastic finite-element method. *Journal of Materials Processing Technology* **1998**, 80-81, 700-706.
19. Berazategui, D.A.; Cavaliere, M.A.; Montelatici, L.; Dvorkin E.N. On the modelling of complex 3D bulk metal forming processes via the pseudo concentrations technique. Application to the simulation of the Mannesmann piercing process. *International Journal for Numerical Methods in Engineering* **2006**, 65, 1113-1144.
20. Shim, S.H.; Cho, J.M.; Lee, M.C.; Joun, M.S. Finite element analysis of a roll piercing process equipped with Diecher's guiding discs. *Transactions of Materials Processing* **2012**, 21, 19-23.
21. Cho, J.M.; Kim, B.S.; Moon, H.K.; Lee, M.C.; Joun, M.S. Comparative study on Mannesmann roll piercing process between Diescher's guiding disk and Stiefel's Guiding Shoe. *AIP Conference Proceedings* **2013**, 1532, 843-849.
22. Joun, M.S.; Lee, J.; Cho, J.M.; Jeong, S.W.; Moon, H.K. Quantitative study on Mannesmann effect in roll piercing of hollow shaft. *Procedia Engineering* **2014**, 81, 197-202.

23. Lee, M.C.; Joun, M.S.; Lee, J.K. Adaptive tetrahedral element generation and refinement to improve the quality of bulk metal forming simulation. *Finite Elements in Analysis and Design* **2007**, 43, 788-802.
24. Lee M.C.; Chung, S.H.; Jang, S.M.; Joun, M.S. Three-dimensional simulation of forging using tetrahedral and hexahedral elements. *Finite Elements in Analysis and Design* **2009**, 45, 745-754.
25. Pater, Z.; Kazanecki, J. Complex numerical analysis of the tube forming process using Diescher mill. *Archives of Metallurgy and Materials* **2013**, 58, 717-724.
26. Skripalenko, M.M.; Bazhenov, V.E.; Romantsev, B.A.; Skripalenko, M.N.; Huy, T.B.; Gladkov, Y.A. Mannesmann piercing of ingots by plugs of different shapes. *Materials Science and Technology* **2016**, 32, 1712-1720.
27. Jung, S.H.; Shin, Y.I.; Song, C.K. Finite element analysis of an elongation rolling process for manufacturing seamless pipes. *Journal of the Korean Society of Precision Engineering* **2014**, 31, 923-928.
28. Xiong, S.; Li, C.S.; Rodrigues, J.M.C.; Martins, P.A.F. Steady and non-steady state analysis of bulk forming processes by the reproducing kernel particle method. *Finite Elements in Analysis and Design* **2005**, 41, 599-614.
29. Topa, A.; Shah, Q.H. Numerical simulations of bulk metal forming process with smooth particle hydrodynamics", *Australian Journal of Basic and Applied Sciences* **2014**, 8, 198-204.
30. Hah, Z.H.; Youn, S.K. Eulerian analysis of bulk metal forming processes based on spline-based meshfree method. *Finite Elements in Analysis and Design* **2015**, 106, 1-15.
31. Schreurs, P.J.G.; Veldpaus, F.E.; Brekelmans, W.M. Simulation of Forming Processes, using the Arbitrary Eulerian-Lagrangian Formulation. *Computer Method in Applied Mechanics and Engineering* **1986**, 58, 19-36.
32. Aymone, J.L.F.; Bittencourt, E.; Creus, G.J. Simulation of 3D metal-forming using an arbitrary Lagrangian–Eulerian finite element method. *Journal of Materials Processing Technology* **2001**, 110, 218-232.
33. Merklein, M.; Koch, J.; Opel, S.; Schneider, T. Fundamental investigations on the material flow at combined sheet and bulk metal forming processes. *CIRP Annals - Manufacturing Technology* **2011**, 60, 283-286.
34. Topa, A.; Shah, Q.H. Failure prediction in bulk metal forming process. *International Journal of Manufacturing Engineering* **2014a**, 2014, 385065, https://doi.org/10.1155/2014/385065.
35. Kronsteiner, J.; Horwatitsch, D.; Zeman, K. Comparison of Updated Lagrangian FEM with Arbitrary Lagrangian Eulerian method for 3D thermo-mechanical extrusion of a tube profile. *AIP Conference Proceedings* **2017**, 1896, 140006.
36. Vavourakis, V.; Loukidis, D.; Charmpis, D.C.; Papanastasiou, P. A robust finite element approach for large deformation elastoplastic plane-strain problems. *Finite Elements in Analysis and Design* **2013**, 77, 1–15.
37. Wang, X.; Li, X. Numerical simulation of three dimensional non-Newtonian free surface flows in injection molding using ALE finite element method. *Finite Elements in Analysis and Design* **2010**, 46, 551-562.
38. Crutzen, Y.; Boman, R.; Papeleux, L.; Ponthot, J.-P. Lagrangian and arbitrary Lagrangian Eulerian simulations of complex roll-forming processes. *Comptes Rendus Mécanique* **2016**, 344, 251-266.
39. Crutzen, Y.; Boman, R.; Papeleux, L.; Ponthot, J.-P. Continuous roll forming including in-line welding and post-cut within an ALE formalism. *Finite Elements in Analysis and Design* **2018**, 143, 11-31.
40. Ducobu, F.; Rivière-Lorphèvre, E.; Filippi, E. Finite element modelling of 3D orthogonal cutting experimental tests with the Coupled Eulerian-Lagrangian (CEL) formulation. *Finite Elements in Analysis and Design* **2017**, 134, 27-40
41. Avevor, Y.; Vincent, J.; Faure, L.; Moufki, A.; Philippon, S. An ALE approach for the chip formation process in high speed machining with transient cutting conditions: Modeling and experimental validation. *International Journal of Mechanical Sciences* **2017**, 130, 546-557.
42. LS-DYNA. *Modeling Guidelines Document*; LS-DYNA Aerospace Working Group (Livermore Software Technology Corporation): Livermore, California, USA, 2013.
43. Chang, K.T.; Brittain, T.M. An investigation of analog materials for the study of deformations in metal processing simulations. *Journal of Engineering for Industry* **1968**, 90, 381-386.
44. Sofuoglu, H.; Rasty, J. Flow behavior of plasticine used in physical modelling of metal forming process. *Tribology International* **2000**, 33, 523-529.
45. Crandall, S.H.; Kurzweil, L.G.; Nigam, A.K. On the measurement of Poisson's ratio for modeling clay. *Experimental Mechanics* **1971**, 11, 402-413.
46. Cross, R. Elastic properties of plasticine, silly putty, and tennis strings. *The Physics Teacher* **2012**, 50, 527-529.

47. Wójcik, Ł.; Lis, K.; Pater, Z. Plastometric tests for plasticine as physical modelling material. *Open Engineering* **2016**, 6, 653-659.
48. Do, I.; Day, J. *LS-DYNA ALE & fluid-structure interaction modeling*; Livermore Software Technology Corporation, Livermore, California, USA, 2005.
49. Nahshon, K.; Hutchinson, J.W. Modification of the Gurson model for shear failure. *European Journal of Mechanics - A/Solids* **2008**, 27, 1-17.